A Comprehensive functional analysis of *NTRK1* missense mutations causing Hereditary Sensory and Autonomic Neuropathy type IV (HSAN IV)

Authors

Samiha S Shaikh

Cambridge Institute for Medical Research, University of Cambridge, Cambridge, UK

Ya-Chun Chen

Cambridge Institute for Medical Research, University of Cambridge, Cambridge, UK

Sally-Anne Halsall

Molecular Genetics Laboratory, Addenbrooke's Hospital, Cambridge, UK

Michael S Nahorski

Cambridge Institute for Medical Research, University of Cambridge, Cambridge, UK

Kiyoyuki Omoto

Neuroscience and Pain Research Unit, Pfizer Ltd, Great Abington, UK

Gareth T Young

Neuroscience and Pain Research Unit, Pfizer Ltd, Great Abington, UK

Anne Phelan (Anne.Phelan@stratifiedmedical.com)

Stratified Medical, 40 Churchway, London, NW1 1LW, UK

Christopher Geoffrey Woods (cw347@cam.ac.uk)

Cambridge Institute for Medical Research, University of Cambridge, Cambridge, CB2 0XY, UK

Corresponding authors

AP and CGW

Grant sponsor

MR/K017551/1

ABSTRACT

Hereditary sensory and autonomic neuropathy type IV (HSAN IV) is an autosomal recessive disorder characterized by a complete lack of pain perception and anhidrosis. Here, we studied a cohort of seven patients with HSAN IV and describe a comprehensive functional analysis of seven novel *NTRK1* missense mutations, c.1550G>A, c.1565G>A, c.1970T>C, c.2096T>C, c.2254T>A, c.2288G>C, c.2311C>T, corresponding to p.G517E, p.G522E, p.L657P, p.I699T, p.C752S, p.C763S and p.R771C, all of which were predicted pathogenic by *in-silico* analysis. The results allowed us to assess the pathogenicity of each mutation and to gain novel insights into TRKA downstream signalling. Each mutation was systematically analyzed for TRKA glycosylation states, intracellular and cell membrane expression patterns, nerve growth factor stimulated TRKA autophosphorylation, TRKA-Y496 phosphorylation, PLCγ activity and neurite outgrowth. We showed a diverse range of functional effects: one mutation appeared fully functional, another had partial activity in all assays, one mutation affected only the PLCγ pathway and four mutations were proved null in all assays. Thus, we conclude that complete abolition of TRKA kinase activity is not the only pathogenic mechanism underlying HSAN IV. By corollary, the assessment of the clinical pathogenicity of HSAN IV mutations is more complex than initially predicted and requires a multifaceted approach.

INTRODUCTION

Pain is a physiological protective mechanism that is essential for the detection and prevention of contact with noxious stimuli present in all multicellular organisms (Dubin and Patapoutian, 2010). Such noxious stimuli are detected by specialized sensory neurons called nociceptors. During development, specification towards a nociceptive phenotype relies on the expression of the receptor called tropomyosin receptor kinase A (TRKA) for the final transition from mitotic precursor to post-mitotic nociceptor (Marmigere and Ernfors, 2007). Further underlining importance of TRKA in human pain, is that either its deficiency or deficiency of its ligand, nerve growth factor (NGF), results in an inherited form of congenital painlessness named Hereditary Sensory and Autonomic Neuropathy type IV (HSAN IV) and HSAN V respectively. In addition, novel antagonists or therapeutic antibodies against NGF-TRKA signalling are showing considerable promise as analgesics in clinical trials (Bannwarth and Kostine, 2014; Spierings *et al.* 2014).

The human TRKA protein is encoded by the gene *NTRK1* (MIM# 191315) located on chromosome 1q21-q22 (Figure 1A). The first isoform of *NTRK1* includes all exons and yields a 796 residue protein that is predominantly expressed in neuronal tissues and provides responsiveness to both NGF and neurotrophin 3 (Barker *et al.* 1993). Exclusion of exon 9 in the second isoform results in a 790 residue protein that is primarily expressed in non-neuronal tissues and binds NGF alone (Barker *et al.* 1993). Previous studies have shown TRKA to be synthesized as an 87 kDa protein, which is immediately glycosylated to a 110 kDa form. Further glycosylation events occur to produce the mature and functional 140 kDa glycoprotein (Martin-Zanca *et al*. 1989), which is then trafficked to the plasma membrane (Watson *et al.* 1999).

The TRKA receptor contains a single transmembrane domain that lies between the extracellular and intracellular domains. The extracellular domain consists of a number of structural motifs (Figure 1B) which specifies binding to NGF, whereas the majority of the intracellular domain comprises a tyrosine kinase domain (Huang and Reichardt, 2003). Intracellular signalling by TRKA is initiated by engagement with an extracellular NGF dimer, which causes the dimerization of two TRKA molecules (Figure 1C) and autophosphorylation of the TRKA kinase domain tyrosine residues Y676, Y680 and Y681 (Cunningham *et al.* 1997). The subsequent structural change allows binding to ATP and results in phosphorylation of Y496 and Y791 (Cunningham and Greene, 1998; Artim *et al.* 2012), which then act as adaptor sites for the downstream signalling molecules Shc and PLCγ respectively, summarized in Figure 1C.

Recruitment of Shc (Dikic *et al.* 1995) and associated adaptor proteins to phosphorylated Y496, activates PI3K to promote neuronal survival (Datta *et al.* 1999; Yuang and Yanker, 2000). Binding of other associated adaptor proteins to Shc activates the Ras/MAPK pathway (Dikic *et al.* 1995; MacDonald *et al.* 2000) (Figure 1C). PLCγ bound to phosphorylated Y791 results in an increase in Ca^{2+} levels and activation of Ca^{2+}/calmodulin-regulated protein kinases (Obermeier *et al.* 1993). The Ras/MAPK and PLCγ pathways converge to lead to transcription of genes that specifically drive neuronal differentiation (Riccio *et al.* 1999; Lonze *et al*. 2002).

HSAN IV (OMIM #256800) is a rare autosomal recessive disorder that is caused by a failure of nociceptive and sympathetic neuron development. One of the characteristic features of HSAN IV is a congenital and complete insensitivity to both superficial and deep painful stimuli. Patients are prone to oral injuries as well as multiple accidental injuries such as burns, falls, and bone and joint fractures (Amano *et al.* 1998; Bar-On *et al.* 2002). Further key features of HSAN IV are a deficit of temperature sensing (Ismail *et al.* 1998; Axelrod

2002) and developmental delay which becomes apparent within the first decade (Rosemberg *et al.* 1994). Recently it has been shown that lack of TRKA signalling increases the susceptibility of patients to infections, in particular to *Staphylococcus aureus*, through a monocyte/macrophage-specific NGF/TRKA pathway (Beiglman *et al.* 2009; Hepburn *et al.* 2014).

Many different mutations have been identified in HSAN IV patients, mostly nonsense mutations, but also missense, small insertions, small deletions and splicing variants. Only a small number of missense mutations have previously been functionally analyzed (review of information in Supp. Table S1), the mutations p.G516R, p.G571R, p.R643W, p.R648C, p.G708S and p.R774P (numbering based on RefSeq ID NP_001012331. All showed diminished kinase activity and absent autophosphorylation (Greco *et al* 1999; Greco *et al.* 2000; Mardy *et al.* 2001; Miranda *et al.* 2002), and in addition, the extracellular domain mutations p.L93P and p.L213P were aberrantly processed and showed reduced kinase activity (Mardy *et al.* 2001; Miranda *et al.* 2002).

We have identified seven novel missense mutations in *NTRK1* from patients with HSAN IV. Extensive functional analysis of each mutation revealed a diverse and novel range of results and suggests multiple pathogenic mechanisms underlie HSAN IV.

METHODS

Molecular genetics, sequencing and segregation studies.

The seven missense mutations described in this study were sequentially ascertained through an NHS genetics service. Patients were accepted for analysis if they had the minimal clinical characteristics of both a congenital pain insensitivity and cognitive delay. Sequencing was by standard Sanger analysis of each exon of *NTRK1* (RefSeq ID NM_002529.3) using a customized set of primers designed to work under identical polymerase chain reaction conditions (primer sequences are available on request). The *NGF* gene (RefSeq ID NM_002506.2) was also sequenced using a set of primers designed to work under identical conditions.

The conservation of the mutated residues was analyzed using the multiple sequence alignment tool Clustl Omega version 1.2.2 (McWilliam *et al.* 2011) (http://www.ebi.ac.uk/Tools/msa/clustalo/). Pathogenicity of mutations was predicted by PolyPhen-2 (Adzhubei *et al.* 2010) (http://genetics.bwh.harvard.edu/pph2/) and by SIFT (Kumar *et al.* 2009) (http://sift.jcvi.org/www/SIFT_enst_submit.html). For all tools, default settings were used. Our chromosome and mutation lab results have been uploaded on DECIPHER (https://decipher.sanger.ac.uk), where they are freely available, under an agreement with NHS-CAM and also on LOVD database (http://grenada.lumc.nl/LSDB_list/lsdbs/NTRK1).

Cloning of expression constructs

The construct for wild-type full length TRKA was obtained from IMAGE clones (Source BioSciences). A C-terminal GFP tagged TRKA construct was generated by introducing full length *NTRK1* cDNA into the pEGFP-N1 cloning vector (Clontech) as described previously

(Mitchell *et al.* 2012), and henceforth referred to as wild-type TRKA-GFP. GFP tagged

TRKA had a similar activity to untagged TRKA (Supp. Figure S1). All the point mutations

were introduced using the QuikChange II Site-directed Mutagenesis Kit (Agilent

Technologies).

Cell culture and conditions

HEK-293, HeLa, and SH-SY5Y cells were cultured in complete DMEM supplemented with

10% FBS, 2 mM L-glutamine and 100 µg/ml penicillin and 100 µg/ml streptomycin, at 37 °C

and 5% CO_2.

For localization studies, HEK-293 cells were plated on poly-L-lysine coated coverslips at a

seeding concentration of $1x10^5$ cells/ml. For neurite outgrowth SH-SY5Y cells were plated

on poly-L-lysine coated coverslips at $5x10^4$ cells/ml. Cells were transiently transfected with

500 ng DNA with Fugene HD transfection reagent (Promega).

For glycosylation assessment, HEK-293 cells were plated at a seeding concentration 2.5 $x10^5$

cells/ml. For phospho-ELISA assays and calcium imaging, HeLa cells were plated at

$1.25x10^5$ cells/ml. For calcium imaging cells were plated on poly-L-lysine coated 35 mm

glass bottom dishes. In all cases cells were transiently transfected with 2.5 µg DNA using

Fugene HD for 24 h.

Colocalization analysis

24 h post-transfection, HEK-293 cells were washed in phosphate buffered saline (PBS) and

fixed in ice-cold methanol. Cells were stained with GFP antibody (Abcam, ab6556, 1:1000)

and Na^+/K^+ ATPase α1 subunit antibody (Abcam, ab7671, 1:300) . Alexa-488 and Alexa-546

conjugated secondary antibodies were purchased from Invitrogen (1:1000). All images were

acquired with an LSM710 laser-scanning META confocal microscope (Carl Zeiss) using a x63 oil-immersion objective.

Image analysis was performed using the Volocity image analysis software (PerkinElmer). Colocalization was quantified in terms of Manders M1 coefficient. The proportion of GFP at the membrane was quantified by measuring the GFP at the plasma membrane and dividing by the total GFP fluorescence.

Glycosylation assessment

Transfected HEK-293 cells were washed with 1x PBS and scraped in RIPA buffer (Tris pH 7.4, NaCl 150 mM, EDTA, 0.5 mM, 1% Triton), containing protease inhibitors (Roche Applied Sciences). Lysates were cleared by centrifugation at 16 000 g at 4 °C for 25 minutes and levels of total cellular protein tested using the DC protein assay kit (BioRad). 25 µg of total protein was treated with PNGase (NEB) following manufacturer's protocol or was left untreated.

PNGase treated and untreated protein lysate were separated using 6% Tris-glycine gels (Invitrogen) and transferred to PVDF membrane (Millipore). Blots were then probed with GFP (D5.1) XP Rabbit mAb #2956 (Cell Signaling Technologies, 1:1000) and lamin antibody (Abcam, ab133741, 1:1000). Secondary antibodies were purchased from Dako and signal was detected using the chemiluminescent HRP substrate (Millipore). Densitometry was performed with ImageJ software (NIH).

Phospho-TRKA assays

24 h post transfection, HeLa cells were serum starved in DMEM supplemented with 1% FBS at 37 °C for 1 h. Cells were then treated with 100 ng/ml NGF (CST) for 5 min at 37 °C or were left untreated and washed in 1x tris buffered saline. Lysate was collected as mentioned

previously, with one alteration: RIPA buffer was supplemented with a 1:100 dilution of phosphatase inhibitor cocktails 2 and 3 (Sigma).

The autophosphorylation and Y496 phosphorylation levels were determined using the PathScan® Phospho-TRKA Sandwich ELISA 674/675 Kit (CST) and PathScan® Phospho-TRKA Tyr490 Sandwich ELISA kit (CST) respectively, following manufacturer's protocol. Total TRKA levels in the lysates were also measured using PathScan® Total TRKA Sandwich ELISA kit (CST).

The relative levels of phosphorylated TRKA were calculated by dividing phosphorylated values by total TRKA values. This was then normalized to the relative phosphorylation of wild-type transfected cells without NGF treatment.

Calcium imaging

24 h post-transfection, calcium imaging was performed on HeLa cells using Rhod-3-AM calcium imaging kit (Invitrogen) following manufacturer's protocol. Images were acquired with an LSM710 laser scanning META confocal microscope (Carl Zeiss) using a x20 objective and maximum pinhole aperture of 600 μm. Two line averages were performed for each frame with images taken every 4 s.

At t= 48 s, 20 μl of HBSS media was added, at t= 140 s, 20 μl NGF (final concentration of 100 ng/ml) was added to the cells. The response to NGF was monitored for 10 min, after which at t= 820 s, 100 ng/ml ionomycin was added. For PLCγ inhibition studies, WT transfected cells were treated with 3 μg/ml of U73122 (Calbiochem) for 30 min prior to NGF stimulation.

Image analysis was performed with the Volocity 3D Image Analysis Software using green cells that did not spontaneously fluoresce and had an ionomycin response.

Neurite outgrowth assays

24 h post transfection, SH-SY5Y cells were treated with 100 ng/ml NGF in DMEM
supplemented with 5% FBS for 9 days, with media being replaced every 3 days. Cells were
then washed in PBS and fixed in 4% paraformaldehyde and were imaged with an LSM510
laser scanning META confocal microscope (Carl Zeiss) using a x40 immersion oil objective.
Cells were analyzed using the ImageJ software. A neurite was identified as being more than
twice the cell body length, where the longest dimension was used (Nahorski *et al.* 2015).
Total neurite length per cell was also quantified where all extensions were measured and
divided by the total number of cells counted (Nahorski *et al.* 2015).

Structural modelling

The homology model of the human TRKA tyrosine kinase domain (UniProtKB: P04629) was
created using in-house Pfizer software and Modeler 9v8 (http://salilab.org/modeller/) (Sali
and Blundell, 1993) using human TRKA structures 4AOJ_A, 4GT5, 4PM, 4PP, 4PS and
4PT, deposited in the Protein Data Bank as templates,
http://www.rcsb.org/pdb/home/home.do, as previously described (Veale *et al.* 2014).

Statistical analysis

The data show the mean ± standard error of the mean (SEM). Statistical significance was
calculated using a one-way ANOVA, followed by unpaired, two sided Student's *t*-test using a
Bonferroni corrected adjusted P-value. Significance was set at *P<0.05, **P<0.01 or
***P<0.001.

RESULTS

Putative mutations in *NTRK1*

Seven cases with a typical HSAN IV phenotype, in which parents had no features of HSAN IV, were referred to the East Anglian NHS Genetics Services for HSAN IV analysis and were sequentially identified. The probands ages were from 3 to 15 years. They had no evidence of having pain or temperature perception, had cognitive global delay ranging from mild to moderate. They did not sweat and usually had icthyotic areas of skin with troublesome puritis. Those over 10 years of age had evidence of Charcot's joints in the lower limbs, and had had at least one significant episode of *S. aureus* infection. (For full clinical and mutation details, see Supp. Table S2.) Four cases were consanguineous, whilst three cases were from singleton families. Through sequencing analysis, we found three individuals who were homozygous for different *NTRK1* mutations, two cases with a heterozygous missense mutation and a heterozygous nonsense mutation and one case with two heterozygous missense mutations. Sequencing of both parents in all cases confirmed that the mutations segregated as expected for an autosomal recessive disorder. *NGF* was also sequenced and contained no mutations. The novel identified mutations were c.1550G>A, c.1565G>A, c.1970T>C, c.2096T>C, c.2254T>A, c.2288G>C, c.2311C>T (RefSeq ID NM_002529.3), corresponding to the TRKA protein changes p.G517E, p.G522E, p.L657P, p.I699T, p.C752S, p.C763S and p.R771C respectively (Figure 1D and Supp. Figure S2). Nucleotide numbering uses +1 as the A of the ATG translation initiation codon in the reference sequence, with the initiation codon as codon 1. There are no variations at these positions recorded in the 1000 Genomes Server, dbSNP (http://www.ncbi.nlm.nih.gov/SNP/), the Exome Variant Server (http://evs.gs.washington.edu/EVS/) or the ExAC database (http://exac.broadinstitute.org). p.G522R (called p.G516R in the paper) has previously been reported in a HSAN IV case (Mardy *et al.* 2001). Interestingly, all of the mutations identified here were located

intracellularly within the kinase domain (Supp. Figure S2 and Supp. Figure S3), as is the case for most of the previously described missense mutations in *NTRK1*. All mutations were in evolutionarily conserved residues and were predicted to be pathogenic by Polyphen and SIFT (Supp. Figure S3). As none of the mutations would be expected to cause a loss of or instability of the TRKA protein, a number of different studies were undertaken to determine the pathogenic mechanism. Table 1 summarizes the results.

Glycosylation changes in TRKA mutants

We first determined whether the mutations affected protein synthesis or post-translational modification. C-terminal tagged GFP wild-type and mutant constructs were transfected into HEK-293 cells and lysates were collected and were either treated with peptide-N-glycosidase (PNGase) or were left untreated. PNGase treatment of wild-type and mutant lysate removed N-glycosylation to yield an unglycosylated backbone of 117 kDa (Figure 2A). Untreated lysate of wild-type TRKA-GFP had two protein bands: the fully glycosylated 170 kDa product and the partially glycosylated 140 kDa product. All of the mutants clearly showed the 170 kDa fully glycosylated and 140 kDa partially glycosylated products. However, compared to wild-type TRKA-GFP, p.L657P showed a 4-fold reduction in the fully glycosylated form, whilst p.I699T and p.R771C showed a 2.5-fold reduction (**$P<0.01$, Figure 2B). p.C763S also showed a 1.3-fold reduction in the 170 kDa form (*$P<0.05$, Figure 2B). p.G517E, p.G522E and p.C752S showed a glycosylation pattern that was similar to wild-type TRKA-GFP.

Localization of TRKA-GFP mutant proteins

We then determined the localization of the mutant TRKA-GFP proteins to see whether the glycosylation changes observed affected the subcellular localization. HEK-293 cells were transfected with wild-type and mutant constructs and were stained with antibodies against

GFP, shown in green, and the plasma membrane marker Na$^+$/K$^+$ ATPase α1 subunit, shown in red (Figure 2C). As previously observed, wild-type TRKA-GFP was present around the periphery of the cells and colocalized with Na$^+$/K$^+$ ATPase staining (Supp. Figure S4). Staining of wild-type TRKA-GFP demonstrated that 45% of the protein was located at the cell surface with the remainder being located intracellularly (Figure 2D). This was not significantly different in cells expressing the p.G517E, p.G522E or p.C752S mutations. Although the remaining mutant proteins colocalized at the plasma membrane, the proportion of GFP at the membrane was significantly reduced to approximately 20% to that of wild-type TRKA-GFP (Figure 2D).

Although many of the mutations altered the glycosylation status of TRKA-GFP and its localization, they did not completely block trafficking of the receptors to the plasma membrane. Therefore, we next questioned whether the mutants could activate various downstream signalling pathways.

Autophosphorylation of TRKA-GFP mutant proteins

We next looked at the effects of the mutations on autophosphorylation of TRKA-GFP. HeLa cells were transfected with wild-type and mutant constructs. The basal level of autophosphorylation of wild-type TRKA-GFP increased 2.5 fold after NGF stimulation (Figure 3A). There was a 3-fold reduction in basal levels of autophosphorylation in four of the mutants, namely p.G522E, p.L657P, p.I699T and p.R771C (***$P<0.001$) and there was no induction of NGF-stimulated TRKA-GFP autophosphorylation (***$P<0.001$, Figure 3A). There were no observable differences in the basal levels of autophosphorylation, nor induction of autophosphorylation after NGF stimulation in p.G517E and p.C752S. In p.C763S there was a 3-fold reduction in basal levels of autophosphorylation and NGF stimulated autophosphorylation (**$P<0.01$).

Y496 phosphorylation of mutant TRKA-GFP proteins

We then looked at the effect of the mutations on Y496 phosphorylation which is important for the recruitment of Shc and downstream signalling through PI3K and the Ras/MAPK pathway. HeLa cells were transfected with wild-type and mutant constructs, and then NGF stimulated. The basal level of wild-type TRKA-GFP Y496 phosphorylation increased 3-fold upon NGF stimulation (Figure 3B). The four mutants, p.G522E, p.L657P, p.I699T and p.R771C, which showed defective autophosphorylation, did not induce Y496 phosphorylation after NGF stimulation (***$P<0.001$), whereas p.G517E and p.C752S did not alter basal nor NGF-stimulated Y496 phosphorylation. In p.C763S there was a 3-fold reduction in basal Y496 phosphorylation and a 2.5-fold reduction in NGF-stimulated Y496 phosphorylation (**$P<0.01$).

Induction of PLCγ pathway

As p.G517E and p.C752S did not seem to have any effect upon trafficking or autophosphorylation, as described above, we determined their ability to activate the PLCγ pathway through monitoring calcium flux after NGF stimulation. We also tested the other mutants. HeLa cells were transfected and loaded with the calcium indicator dye rhodamine-3. In wild-type transfected cells, after NGF stimulation, there was an increase in basal fluorescence (Figure 4A) to a maximum fluorescence of 2.5 AU at t = 208s (Supp. Figure S5A). Furthermore, 90% of transfected cells responded to NGF (Supp. Figure S5B). Treatment with U73122, a PLCγ inhibitor, abolished induction of NGF increase of calcium (Supp. Figure S5C).

Fluorescence remained at basal levels in cells transfected with the mutant proteins that did not autophosphorylate or phosphorylate Y496 (Supp. Figure S5A). NGF stimulation of p.G517E transfected cells did not induce an increase in red fluorescence (Figure 4B), which

remained at basal levels (**$P<0.01$) and the percentage of cells responsive to NGF was 3% (Supp. Figure S5B). There was no observable difference in the calcium response in p.C752S transfected cells (Figure 4C) compared to the response observed in wild-type TRKA-GFP proteins. In p.C763S transfected cells, basal fluorescence increased to a maximum value of 1.2 AU (Figure 4D, **$P<0.01$) and only 50% of cells were NGF responsive.

Neurite outgrowth

Activation of the different signalling pathways triggered by TRKA ultimately results in differentiation towards a neuronal phenotype (Huang and Reichardt, 2003). Consequently, we looked at the effect of selected mutations on induction of neuronal differentiation. The neuroblastoma cell line SH-SY5Y was transfected with wild-type TRKA-GFP, the mutants p.G517E, p.L657P, p.C752S, p.C763S and empty vector and treated with NGF over nine days (Figure 5A).

After nine days of NGF stimulation, 40% of cells transfected with wild-type TRKA-GFP differentiated into a neuronal phenotype (Figure 5B) and the average neurite length was 360 AU (Figure 5C). Although there was a significant reduction in the percentage of differentiated p.G517E transfected cells (***$P<0.001$), the average neurite length was not significantly different. p.C752S did not affect neurite outgrowth nor neurite length. The p.C763S mutation resulted in a significant reduction in the percentage of differentiated cells to 20% (***$P<0.001$) and a significant reduction of neurite length (***$P<0.001$). p.L657P was included as a negative control and only 5% of transfected cells could be classified as differentiated, which resembles the percentage of spontaneous differentiated cells in the empty transfected control.

Structural modelling of TRKA mutations

We next modelled the structural consequences of the mutations on the kinase domain (Supp. Figure S2, Supp. Figure S3C). We found that p.G517 and p.G522 are the first and third glycine residues within the ATP binding domain GxGxxG. Ligand binding and autophosphorylation of TRKA induce a conformational change that shifts TRKA into an open conformation and allows binding of ATP which increases the kinase activity (Jullien *et al.* 2002). p.L657 is structurally within the active site of TRKA, where it is likely to have a stabilization role. p.I699 is within the activation loop, which is essential for autophosphorylation and hence may have a role in enabling autophosphorylation to occur. p.C752, p.C763 and p.R771 are all within the catalytic domain of TRKA and hence are likely to affect activity of TRKA.

DISCUSSION

In this study we report seven novel missense mutations found in patients with a HSAN IV phenotype. We have undertaken a comprehensive assessment of the effects of each of these mutations on TRKA function, using a greater range of methods than has been previously reported (Greco *et al.* 1999; Greco *et al.* 2000; Mardy *et al.* 2001; Miranda *et al.* 2002): glycosylation and membrane expression, autophosphorylation, Y496 phosphorylation, PLCγ activation and effects on neurite outgrowth (summarized in Table 1).

Glycosylation of TRKA is essential for its function and thus we assayed this for each of our mutations. p.G517E showed a similar glycosylation pattern to wild-type TRKA-GFP. We observed no changes in subcellular localization for this mutant protein as full glycosylation is required for trafficking to the plasma membrane (Watson et al 1999). p.G517E did not affect autophosphorylation and as a result downstream phosphorylation of Y496 was found to be unaffected. However, the p.G517E mutation completely abolished PLCγ signalling and we found that the mutation was less efficient at promoting differentiation and neurite outgrowth. p.G517E is the first glycine in the ATP binding domain GxGxxG. Hence it is surprising that Y496 phosphorylation is observed and PLCγ signalling is abolished. The attenuation of PLCγ signalling may be due a conformational change within the kinase domain that alters PLCγ signalling. This is the first mutation identified within the kinase domain that does not alter kinase activity of TRKA. It is also the first mutation identified to date that only affects one signalling pathway and yet is sufficient to restrict differentiation and thus must be the pathogenic mechanism behind HSAN IV. The result highlights the fact that when assessing the pathogenicity of TRKA patient mutations, it is not sufficient to just look at autophosphorylation or Y496 phosphorylation as has been done previously (Greco *et al* 1999; Greco *et al.* 2000; Mardy *et al.* 2001; Miranda *et al.* 2002). Clinically the patient with

p,G517E mutation had typical HSAN IV phenotype and was indistinguishable from our other cases.

p.G522E mutation also showed a similar glycosylation pattern to wild-type TRKA and hence no differences in membrane expression were observed. There was no induction of TRKA autophosphorylation after NGF stimulation. As a consequence of a lack of TRKA activation, downstream signalling through Y496 and PLCγ were abolished. As this mutant protein retains membrane localisation, it is likely that the primary pathogenic mechanism is absent intrinsic kinase activity. The effect of this mutation is unexpected because p.G522E resides within the ATP binding domain and autophosphorylation is not dependent on ATP binding. Hence it appears that G522 may function directly in kinase activity and changes to the structure of the kinase domain leads to no kinase function. This is confirmed by studies on a different mutation at this site, p.G522R (termed p.G516R in the paper) where the mutation also rendered the protein kinase-dead (Mardy *et al.* 2001).

p.L657P, p.I699T, and p.R771C all exhibited similar results in the assays performed. We found a decrease of fully glycosylated TRKA-GFP in these mutant proteins and the partially glycosylated 140 kDa product was favoured. We hypothesized this effect may be explained by mutation-induced conformational changes that alter the accessibility of enzymes to the glycosylation sites. An alternative explanation could be that these mutations cause aberrant folding of the TRKA kinase domain, that may be detected by cellular proofing systems and start degrading these mutants even before they become fully glycosylated. Furthermore, these mutations had more TRKA-GFP protein in the cytoplasm than at the plasma membrane, confirming previous results that trafficking to the plasma membrane is related to glycosylation status. However, as there was some TRKA-GFP at the membrane for each of these mutations, we next sought to investigate downstream signalling pathways. In all cases TRKA-GFP autophosphorylation was abolished. Neurite outgrowth in p.L657P (as a

representative) was also abolished. As the four kinase-dead mutants retained some membrane localization it is likely that the primary pathogenic mechanism is absent intrinsic kinase activity. Structural modelling showed that p.G522E, p.L657P, p.I699T and p.R771C were located in important parts of the kinase domain: the ATP binding domain, active site, activation loop and the catalytic domain respectively. It is likely that the mutations introduce a change to the 3D structure of the kinase domain which would lead to a lack of kinase activity. As such, it is unsurprising that autophosphorylation is affected and our results confirm that these residues have an essential role in autophosphorylation. These results are similar to those published previously where most the missense mutations were found to produce kinase-dead mutants (Greco *et al* 1999; Greco *et al.* 2000; Mardy *et al.* 2001; Miranda *et al.* 2002).

C752S did not affect glycosylation and hence did not affect trafficking to the membrane. In addition, autophosphorylation, Y496 phosphorylation and PLCγ activation were unaffected. Furthermore, neurite outgrowth data indicated that the mutation did not affect differentiation. p.C752S is within the catalytic domain but we could find no evidence of disrupted function. This heterozygous mutation was found *in-trans* with the heterozygous kinase-dead p.G522E mutation and no other *NTRK1* change was detected despite complete Sanger sequencing. Furthermore, the nucleotide change was not predicted to change or create a splice site. Thus it appears that even though this mutation affects an evolutionary conserved residue, it is not pathogenic and in fact could be a rare but harmless polymorphism. In this family we have failed to discover the other pathogenic mutation in *NTRK1*. The C752S result highlights the weakness of *in silico* predictions of pathogenicity and indicates functional work is necessary to call for pathogenic mutations.

p.C763S is within the catalytic domain and only partially reduced both autophosphorylation and consequently Y496 phosphorylation. Nonetheless this is sufficient to cause disease. This

suggests that there is an essential level of activation of TRKA required before nociceptor differentiation can take place. As we found this patient to be phenotypically indistinguishable from our other HSAN IV cases, it must be concluded that the mutations renders the TRKA signal insufficient to trigger differentiation. This is the first reported case where a reduction in TRKA signalling, but not abolition, leads to a HSAN IV phenotype.

In conclusion, we report seven novel *NTRK1* mutations in individuals with a diagnosis of HSAN IV, and have found evidence to support pathogenicity in six. Our results highlight the fact that when assessing the pathogenicity of TRKA mutations (for example p.G517E), it is not sufficient to only assess autophosphorylation or Y496 phosphorylation, as has been done previously (Greco *et al* 1999; Greco *et al.* 2000; Mardy *et al.* 2001; Miranda *et al.* 2002). Similarly complete evolutionary conservation is also not an absolute predictor of pathogenicity, as we found no evidence that p.C752S was pathogenic, confirming the need for caution when interpreting the pathogenicity of unknown variants (Waxman *et al.* 2014). Our data highlights the complexity of TRKA function and suggests that perturbation of any part of the downstream signalling may lead to a loss of nociceptor development.

CONFLICT OF INTEREST

The authors declare no conflict of interest.

REFERENCES

Amano A, Akiyama S, Ikeda M, Morisaki I 1998. Oral manifestations of hereditary sensory and autonomic neuropathy type IV. Congenital insensitivity to pain with anhidrosis. Oral Surg Oral Med Oral Pathol Oral Radiol Endod 86:425-431

Artim SC, Mendrola JM, Lemmon MA 2012. Assessing the range of kinase autoinhibition mechanisms in the insulin receptor family. Biochem J 448:213-220

Axelrod FB 2002. Hereditary sensory and autonomic neuropathies. Familial dysautonomia and other HSANs. Clin Auton Res 12(Suppl 1):12-14

Adzhubei IA, Schmidt S, Peshkin L, Ramensky VE, Gerasimova A, Bork P, Kondrashov AS, Sunyaev SR 2010. A method and server for predicting damaging missense mutations. Nat Methods 7:248-249

Bannwarth B, Kostine M. Targeting nerve growth factor (NGF) for pain management: What does the future hold for NGF antagonists? 2014. Drugs 74:619-626

Barker PA, Lomen-Hoerth C, Gensch EM, Meakin SO, Glass DJ, Shooter EM 1993. Tissue-specific alternative splicing generates two isoforms of the trkA receptor. J Biol Chem 268:15150-15157

Bar-On E, Weigl D, Parvari R, Katz K, Weitz R, Steinberg T 2002. Congenital insensitivity to pain. Orthopedic manifestations. J Bone Joint Surg Br 84:252-257

Beiglman A, Levy J, Hadad N, Pinsk V, Haim A, Fruchtman Y, Levy R 2009. Abnormal neutrophil chemotactic activity in children with congenital insensitivity to pain with anhidrosis (CIPA): the role of nerve growth factors. Clin Immunol 130:365-72

Cunningham ME, Stephens RM, Kaplan DR, Greene LA 1997. Autophosphorylation of activation loop tyrosine regulates signaling by the TRK nerve growth factor receptor. J Biol Chem 272:10957-10967

Cunningham ME, Greene LA 1998. A function-structure model for NGF-activated Trk. EMBO J 17:7282-7293

Datta SR, Brunet A, Greenberg ME 1999. Cellular survival: a play in three Akts. Genes Dev 13:2905-2927

Dikic I, Batzer AG, Blaikie A, Obermeier A, Ullrich A, Schlessinger J, Margolis M 1995. Shc binding to nerve growth factor receptor is mediated by the phosphotyrosine interaction domain. J Biol Chem 270:15125-15129

Dubin A, Patapoutian A 2010. Nociceptors: the sensors of the pain pathway. J Clin Invest 120:3760-3772

Greco A, Villa R, Tubino B, Romano L, Penso D, Pierotti MA 1999. A novel NTRK1 mutation associated with congenital insensitivity to pain with anhidrosis. Am J Hum Genet 64:1207-1210

Greco A, Villa R, Fusetti L, Orlandi R, Pierotti 2000. The Gly571Arg mutation, associated with the autonomic and sensory disorder congenital insensitivity to pain with anhidrosis, causes the inactivation of the Ntrk1/ nerve growth factor receptor. J Cell Physiol 182:127-133

Hepburn L, Prajsnar TK, Klapholz C, Moreno P, Loynes CA, Ogryzko NV, Brown K, Shiebler M, Hegyi K, Antrobus R, Hammond KL, Connolly J et al. 2014. Innate immunity. A Spaetzle-like role for nerve growth factor β in vertebrate immunity to Staphylococcus aureus. Science 346:641-646

Huang EJ, Reichardt LF 2003. Trk receptors: roles in signal transduction. Annu Rev Biochem 72:609-642

Ismail EA, Al-Shammari N, Anim JT, Moosa A 1998. Congenital insensitivity to pain with anhidrosis: lack of eccrine sweat gland innervation confirmed. J Child Neurol 13:243-246

Jullien J, Guili V, Reichardt LF, Rudkin BB 2002. Molecular kinetics of nerve growth factor receptor trafficking and activation. J Biol Chem 277:38700-38708

Kumar P, Henikoff S, Ng PC 2009. Predicting the effects of coding non-synonymous variants on protein function using the SIFT algorithm. Nat Protoc 4:1073-81

Lonze BE, Riccio A, Cohen S, Ginty DD 2002. Apoptosis, axonal growth defects, and degeneration of peripheral neurons in mice lacking CREB. Neuron 34:371-385

McWilliam H, Li W, Uludag M, Squizzato S, Park YM, Buso N, Cowley AP, Lopez R 2013. Analysis tool web services from the EMBL-EBI. Nucl Acids Res 41:597-600

MacDonald JIS, Gryz EA, Kubi CJ, Verdi JM, Meakin SO 2000. Direct binding of the signaling adapter protein Grb2 to the activation loop tyrosines on the nerve growth factor receptor tyrosine kinase, TRKA. J Biol Chem 275:18225-18223

Mardy S, Miura Y, Endo F, Matsuda I, Indo Y 2001. Congenital insensitivity to pain with anhidrosis (CIPA): effect of TRKA (NTRK1) missense mutations on autophosphorylation of the receptor tyrosine kinase for nerve growth factor. Hum Mol Genet 10:179-188

Marmigere F, Ernfors P 2007. Specification and connectivity of neuronal subtypes in the sensory lineage. Nat Rev Neurosci 8:14-127

Martin-Zanca D, Oskam R, Mitra G, Copeland T, Barbacid M 1989. Molecular and biochemical characterization of the human trk proto-oncogene. Mol Cell Biol 9:24-33

Miranda C, Virgilio MD, Selleri S, Zanotti G, Pagliardini S, Pierotti MA, Greco A 2002. Novel pathogenic mechanisms of congenital insensitivity to pain with anhidrosis genetic disorder unveiled by functional analysis of neurotrophic tyrosine receptor kinase type 1/ nerve growth factor receptor mutations. J Biol Chem 277:6455-6462

Mitchel DJ, Blasier KR, Jeffery ED, Ross MW, Pullikuth AK, Suo D, Park J, Smiley WR, Lo KW, Shabanowitz J, Deppmann CD, Trinidad JC et al. 2012. Trk activation of the ERK1/2 Kinase pathway stimulates intermediate chain phosphorylation and recruits cytoplasmic dynein to signaling endosomes for retrograde axonal transport. J Neurosci 32:15495-15510

Nahorski MS, Al-Gazali L, Hertecant J, Owen DJ, Borner GH, Chen YC, Benn CL, Carvalho OP, Shaikh SS, Phelan A, Robinson MS, Royle SJ, Woods CG 2015. A novel disorder reveals clathrin heavy chain-22 is essential for human pain and touch development. Brain 138:2147-2160

Obermeier A, Halfter H, Wiesmuller KH, Jung G, Schlessinger J, Ullrich A 1993. Tyrosine 785 is a major determinant of Trk-substrate interaction. EMBO J 12:933-941

Riccio A, Ahn S, Davenport CM, Blendy JA, Ginty DD 1999. Mediation by a CREB family transcription factor of NGF-dependent survival of sympathetic neurons. Science 286:2358-2361

Rosemberg S, Marie SK and Kliemann S 1994. Congenital insensitivity to pain with anhidrosis (hereditary sensory and autonomic neuropathy type IV). Pediat Neurol 11:50-56

Sali A, Blundell TL. Comparative protein modelling by satisfaction of spatial restraints 1993. J Mol Biol 234:779-815

Spierings EL, Fidelholtz J, Wolfram G, Smith MD, Brown MT, West CR. 2014. A phase III placebo- and oxycodone-controlled study of tanezumanb in adults with osteoarthritis pain of the hip or knee: response. Pain 155:2432-2333

Veale EL, Al-Moubarak E, Bajaria N, Omoto K, Cao L, Tucker SJ, Stevens EB, Mathie A 2014. Influence of the N terminus on the biophysical properties and pharmacology of TREK1 potassium channels. Mol Pharmacol 85:671-81

Watson FL, Porcionatto AM, Bhattacharyya A, Stiles CD, Segal RA 1999. TRKA glycosylation regulates receptor localization and activity. J Neurobiol 39:323-36

Waxman SG, Merkies IS, Gerrits MM, Dib-Hajj SD, Lauria G, Cox JJ, Wood JN, Woods CG, Drenth JP, Faber CG 2014. Sodium channel genes in pain-related disorders: phenotype-genotype associations and recommendations for clinical use. Lancet Neurol 13:1152-1160

Yuang J, Yankner BA 2000. Apoptosis in the nervous system. Nature 407:802-809

LEGENDS TO FIGURES

Figure 1: TRKA structure, signalling and Identification of novel *NTRK1* mutations in patients with HSAN IV

(A): *NTRK1* located on chromosome 1q21-q22, shown by the grey bar on the ideogram, consists of 17 exons and spans region of 25 kb. Inclusion of all 17 exons encodes for the neuronal specific isoform of TRKA.

(B): The extracellular domain of TRKA consists of a number of structural domains: a leucine rich repeat, flanked on either side by a cysteine rich domain, and two immunoglobulin-like domains. The majority of the intracellular domain comprises the kinase domain.

(C): Signalling through TRKA is initiated through NGF binding, TRKA dimerization, and autophosphorylation of Y676, Y680 and Y681. Subsequent phosphorylation of Y496 and Y791 leads to activation of downstream signalling cascades which drive neuronal differentiation and survival.

(D): Seven individuals were ascertained with a standard HSAN IV phenotype. The identified mutations were p.G517E, p.G522E, p.L657P, p.I699T, p.C752S, p.C763S and p.R771C. Only the exons that code for the kinase domain are shown. TKD: tyrosine kinase domain.

Figure 2: Expression, processing and localization of wild-type and mutant TRKA

(A): Expression of C-terminal GFP tagged wild-type and mutant TRKA constructs in transfected HEK-293 cells. The lanes "+" and "-" represent lysates treated

with/without PNGase respectively. Lamin B1 was included as a loading control. Representative image of n= 3 is shown. WT: wild-type, EV: empty vector.

(B): Quantification of relative levels of fully glycosylated 170 kDa TRKA-GFP protein to the levels of partially glycosylated 130 kDa TRKA-GFP protein.

(C): Localization of TRKA-GFP wild-type and mutant proteins in transfected HEK-293 cells. The cells were stained against GFP (green) and the plasma membrane marker Na^+/K^+ ATPase (red). Wild-type TRKA and all the mutants show membrane expression.

(D): Relative levels of GFP at the membrane compared to the levels of GFP in the cytoplasm. Graph represents mean values of n= 3, with at least 15 cells in each repeat, and error bars represent standard error of the mean.

Statistical differences are indicated as *$P<0.05$, **$P<0.01$ (one-way ANOVA, followed by Student's t test using a Bonferroni adjusted P-value).

Figure 3: Relative Y680/681 and Y496 phosphorylation of mutant TRKA

(A): Basal level of wild-type and mutant TRKA-GFP autophosphorylation in transfected untreated HeLa cells. Response to wild-type and mutant TRKA-GFP protein to 15 min stimulation with 100 ng/ml NGF.

(B): Basal level of Y496 phosphorylation in wild-type and mutant TRKA proteins in untreated cells and after NGF stimulation.

The bar graphs in A and B represents the mean values of n= 3 and error bars represents standard error of the mean. Statistical differences between induced phosphorylation of wild-type and mutant TRKA are indicated as **$P<0.01$ or

***P<0.001 (one-way ANOVA, followed by Student's t test using a Bonferroni adjusted P-value). WT: wild-type; EV: empty vector

Figure 4: Effect of mutations on induction of PLCγ pathway

(A): HeLa cells were transfected with wild-type and mutant TRKA constructs and loaded with rhodamine-3 and response to NGF was monitored. Ionomycin was used as the positive control. Only cells that did not spontaneously fluoresce and had an ionomycin response were used for analysis. WT: wild-type.

(B): No significant increase in calcium levels was observed after NGF stimulation in p.G517E transfected cells.

(C): There was an increase in fluorescence in p.C752S transfected cells which peaked at t= 208.

(D): NGF stimulation on cells transfected with p.C763S caused an increase in fluorescence but the maximum value was reduced.

Figure 5: Differentiation ability of selected mutants

(A): Representative images of transfected SH-SY5Y cells treated with NGF for 9 days. WT: wild-type, EV: empty vector. Green signal indicates transfected cells, blue DAPI nuclear stain.

(B): Quantification of percentage of neurite bearing cells. A neurite was defined as being two times the cell body length.
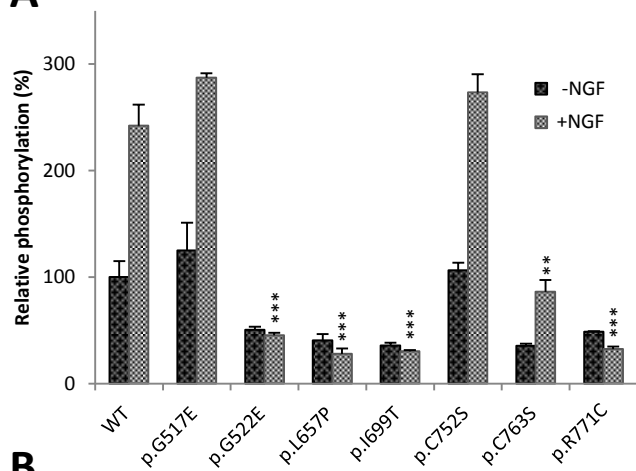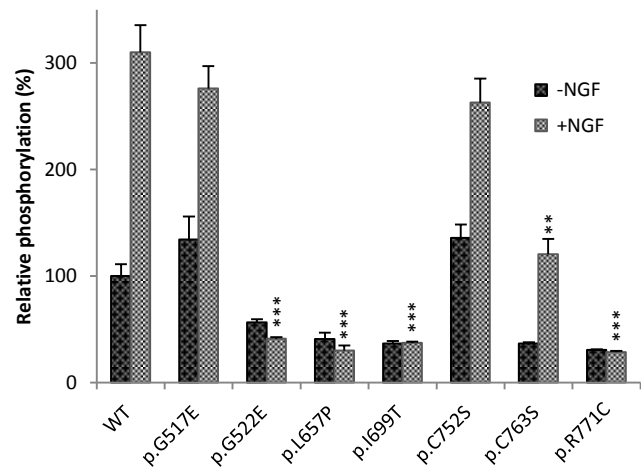
(C): Average neurite length was also quantified. For this all extensions however small were measured.

The bar graphs in B and C represent the mean values of n= 3, with 60 cells in each repeat, and error bars represent standard error of the mean. Statistical differences are indicated as **P<0.01 or ***P<0.001 (one-way ANOVA, followed by Student's t test using a Bonferroni adjusted P-value).

A Chr1 (q23.1)

Gene

B Protein
SP | Cys | LRR | Cys | IgC1 | IgC2 | TM | TKD

C

NGF NGF TRKA

Plasma membrane

PI3K Gab Grb Shc P — Y496 — P Shc Grb Sos Ras ····> PI3K

AKT/PKB

Y680 P
Y681 P
Y791 P PLCγ Ca²⁺ PKC

Neuronal survival

MAPK cascade

Neurite outgrowth

D

Gene
13 14 15 16 17

Protein
TKD

p.G517E p.G522E p.L657P p.I699T p.C763S
p.C752S p.R771C
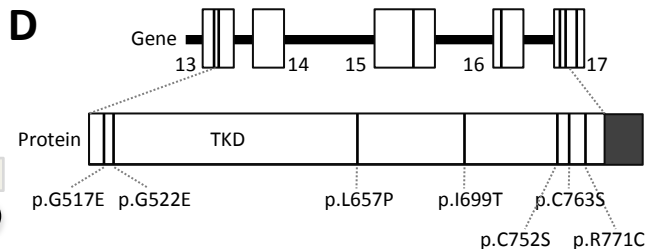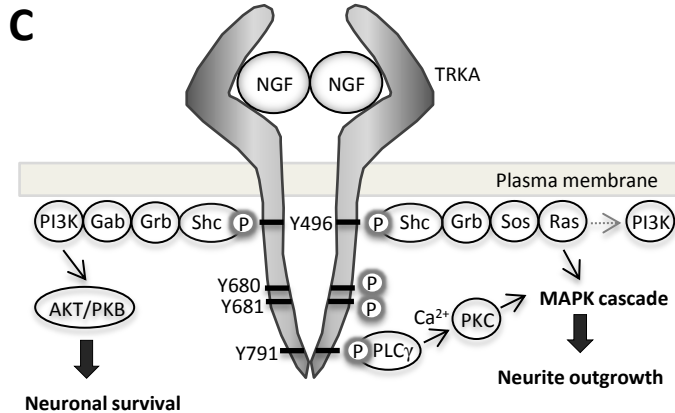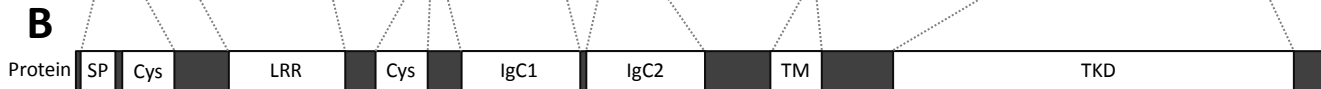
Key:
SP: signal peptide
Cys: cystein rich domain
LRR: leucine rich repeat
IgC: immunoglobulin-like domain
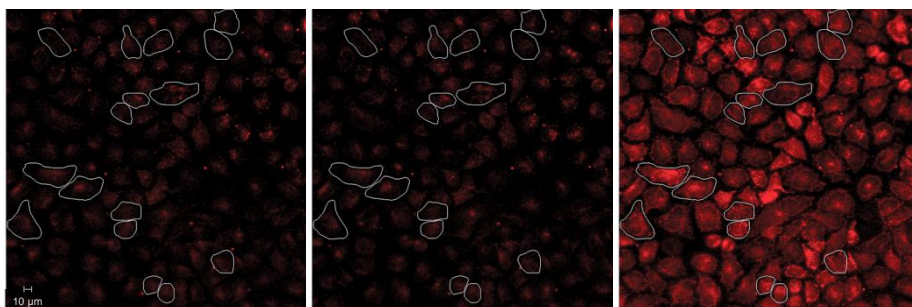TM: transmembrane domain
TKD: tyrosine kinase domain

A

kDa   WT   p.G517E   p.G522E   p.L657P   p.I699T   p.C752S   p.C763S   p.R771C   EV

− + | − + | − + | − + | − +   − + | − + | − + | − +   PNGase

250   GFP

130

95

70   Lamin

B

Relative intensity (AU)

1.6

1.2

0.8

0.4

0

WT   p.G517E   p.G522E   p.L657P**   p.I699T**   p.C752S   p.C763S*   p.R771C**

C

WT   p.G517E

p.G522E   p.L657P

p.I699T   p.C752S

p.C763S   p.R771C

10 µm

D

Relative fluorescence (AU)

1.6

1.2

0.8

0.4
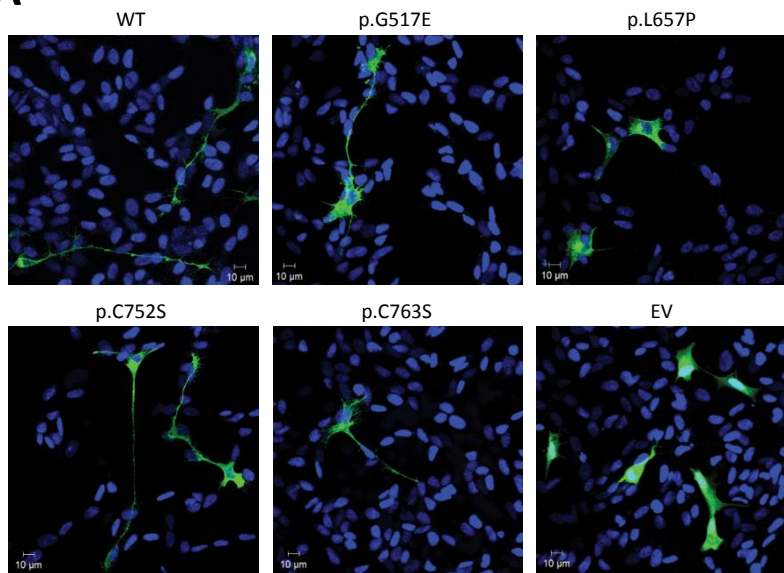
0

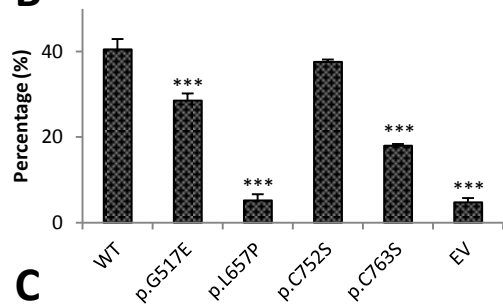WT   p.G517E   p.G522E   p.L657P***   p.I699T***   p.C752S   p.C763S***   p.R771C***
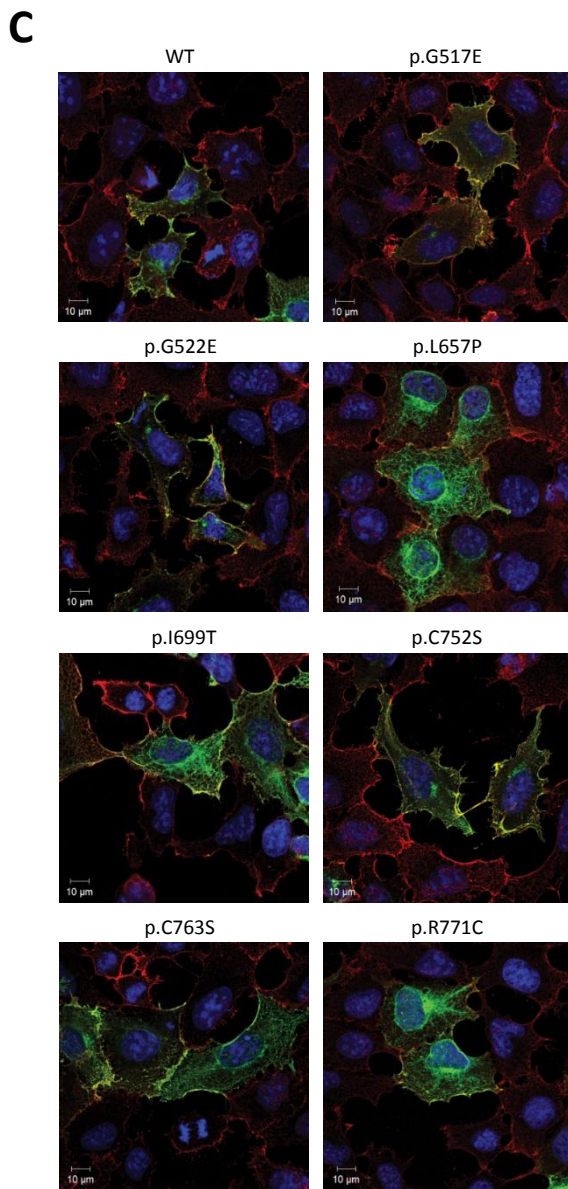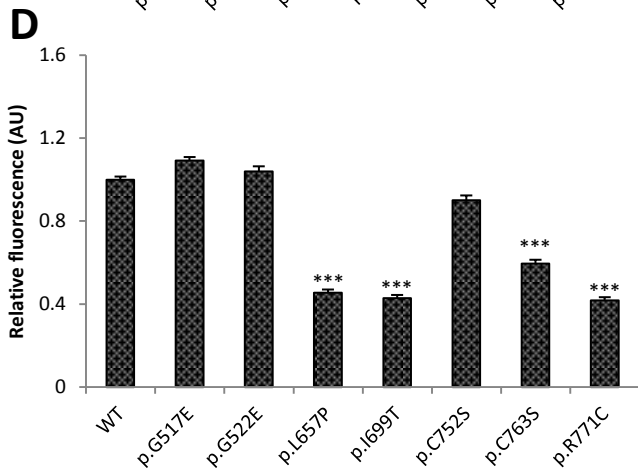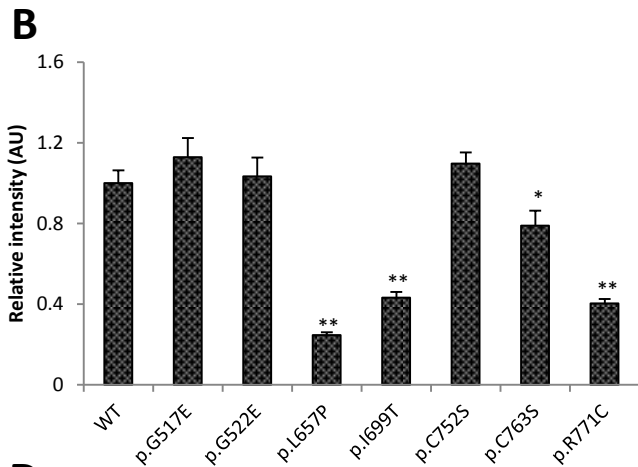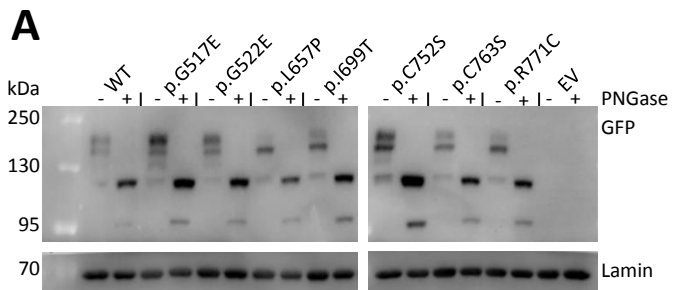
	Pre-NGF application	Post-NGF application	Post-ionomycin application	
A				WT
B				p.G517E
C				p.C752S
D				p.C763S

A

WT p.G517E p.L657P

p.C752S p.C763S EV

B

Percentage (%)

WT p.G517E p.L657P p.C752S p.C763S EV

C

Neurite length (AU)

WT p.G517E p.L657P p.C752S p.C763S EV

A

A

A

p.G517E	LKWEL**E**EGAFG
H. sapiens	LKWEL**G**EGAFG
X. laevis	LKREL**G**EGAFG
D. rerio	LKWEL**G**EGAFG
G. gallus	LKWEL**G**EGAFG
D. melanogaster	FLEEL**G**EGAFG
C. elegans	VREKI**G**EGQFG

p.G522E	GEGAF**E**KVFLA
H. sapiens	GEGAF**G**KVFLA
X. laevis	GEGAF**G**KVFLA
D. rerio	GEGAF**G**KVYLA
G. gallus	GEGAF**G**KVFLA
D. melanogaster	GEGAF**G**KVYkG
C. elegans	GEGQF**G**VVHSG

p.L657P	ATRNC**P**VGQGL
H. sapiens	ATRNC**L**VGQGL
X. laevis	ATRNC**L**VGENL
D. rerio	ATRNC**L**VGEGL
G. gallus	ATRNC**L**VGHDL
D. melanogaster	AARNC**L**VNEGL
C. elegans	ATRNC**L**VGDTR

p.I699T	MPPEST**T**LYRKF
H. sapiens	MPPES**I**LYRKF
X. laevis	MPPES**I**MYRKF
D. rerio	MPPES**I**MYRKF
G. gallus	MPPES**I**LYRKF
D. melanogaster	MPSES**I**LYGKF
C. elegans	MSKEA**I**EQGRF

p.C752S	ERPRA**S**PPEVY
H. sapiens	ERPRA**C**PPEVY
X. laevis	QRPRT**C**PKEVY
D. rerio	ERPRT**C**PKEVH
G. gallus	ERPRT**C**PSEVY
D. melanogaster	SAPEN**C**PTAVY
C. elegans	ECPHN**C**PTNIY

p.C763S	AIMRG**S**WQREP
H. sapiens	AIMRG**C**WQREP
X. laevis	ALMRG**C**WQREP
D. rerio	LLMQG**C**WQREP
G. gallus	DIMQS**C**WQREP
D. melanogaster	SLMIE**C**WHEQS
C. elegans	SLMVE**C**WHENI

| p.R771C	KDVHA**C**LQALA
H. sapiens	KDVHA**R**LQALA
X. laevis	KEIHS**L**LQNLS
D. rerio	KDIYS**R**LVALV
G. gallus	QDIHS**R**LQALV
D. melanogaster	TDISN**R**LKTWH
C. elegans	SEIRS**R**LQSWS

B

Mutation	SIFT prediction score	Polyphen prediction score
p.G517E	0.00	1.000
p.G522E	0.00	1.000
p.L567P	0.00	0.983
p.I699T	0.00	0.953
p.C752S	0.00	1.000
p.C763S	0.00	1.000
p.R771C	0.00	1.000

C

```
481 GKGSGLQGHIIENPQYFSDACVHHIKRRDIVLKWELGEGA
521 FGKVFLAECHNLLPEQDKMLVAVKALKEASESARQDFQRE
561 AELLTMLQHQHIVRFFGVCTEGRPLLMVFEYMRHGDLNRF
601 LRSHGPDAKLLAGGEDVAPGPLGLGQLLAVASQVAAGMVY
641 LAGLHFVHRDLATRNCLVGQGLVVKIGDFGMSRDIYSTDY
681 YRVGGRTMLPIRWMPPESILYRKFTTESDVWSFGVVLWEI
721 FTYGKQPWYQLSNTEAIDCITQGRELERPRACPPEVYAIM
761 RGCWQREPQQRHSIKDVHARLQALAQAPPVYLDVLG
```
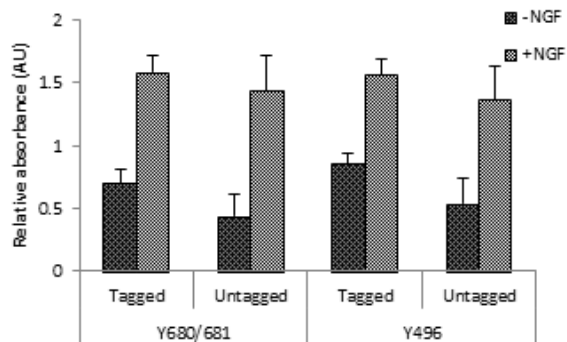
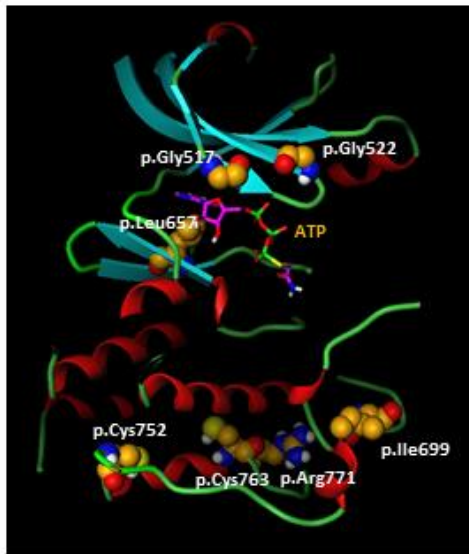| ATP binding domain	Activation loop
Active site	Catalytic domain

A
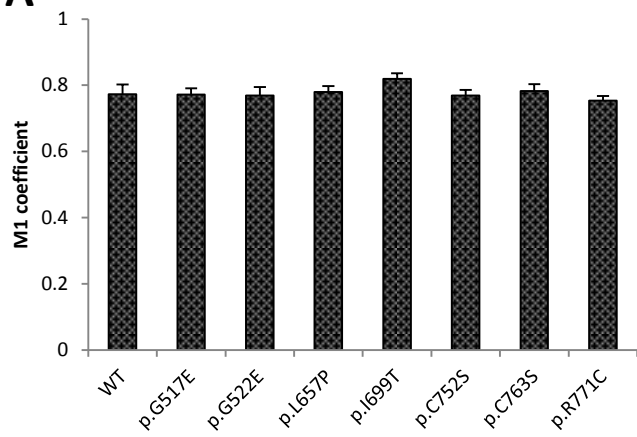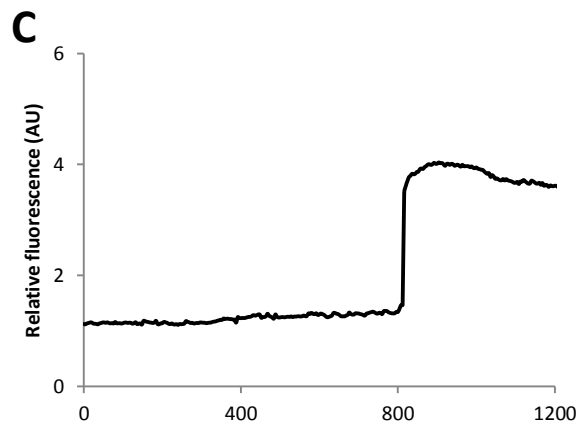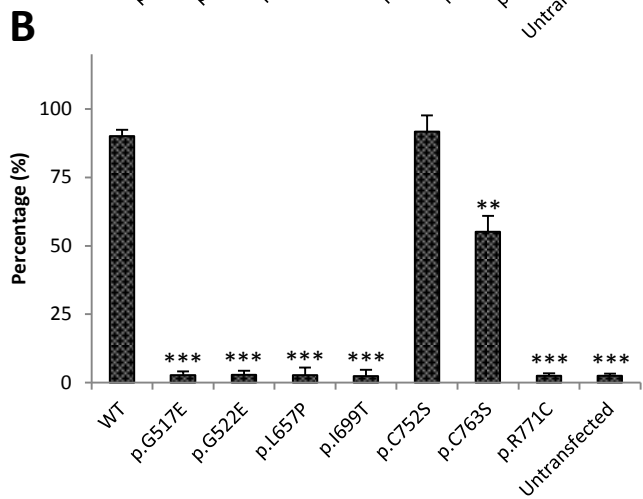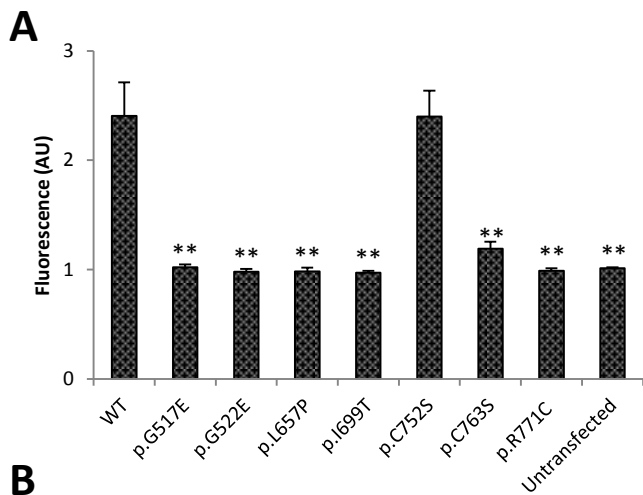
Supplementary Figure S1: Activity of GFP-tagged and untagged wild-type TRKA

To test whether the introduction of GFP at the C-terminus of TRKA affected its function, we introduced the stop codon, TAG, into the construct using site directed mutagenesis and introduction of the mutation was confirmed by sequencing. HeLa cells were then transfected with the two different constructs, and were treated with NGF or were left untreated. Y680/681 autophosphorylation and Y496 phosphorylation were determined by ELISA. There was no observable differences in the basal levels of autophosphorylation or Y496 phosphorylation in cells transfected with GFP-tagged and untagged constructs (P= 0.40, P= 0.37, respectively, n= 3, Student's t test). Furthermore, NGF-induced autophosphorylation and Y496 phosphorylation were not different in cells transfected with GFP-tagged and untagged constructs (P= 0.85, P= 0.90, respectively, n= 3, Student's t test).

Supplementary Figure S2: TrkA structure and position of mutated residues

According to the structural model of the kinase domain of TRKA, p.G517, p.G522 and p.L657, located in the ATP binding domain and the active site, are in close proximity to ATP. Any alteration to these residues is likely to interfere with interaction with ATP and may lead to structural alterations. p.I699 is located within the activation loop and the three remaining residues are within the catalytic domain and possibly are required for substrate binding.

Supplementary Figure S3: Alignment and conservation of mutated residues

A

p.G517E   LKWELEEGAFG
H. sapiens   LKWELGEGAFG
X. laevis   LKRELGEGAFG
D. rerio   LKWELGEGAFG
G. gallus   LKWELGEGAFG
D. melanogaster   FLEELGEGAFG
C. elegans   VREKIGEGQFG

p.G522E   GEGAFEKVFLA
H. sapiens   GEGAFGKVFLA
X. laevis   GEGAFGKVFLA
D. rerio   GEGAFGKVYLA
G. gallus   GEGAFGKVFLA
D. melanogaster   GEGAFGKVYkG
C. elegans   GEGQFGVVHSG

p.L657P   ATRNCPVGQGL
H. sapiens   ATRNCLVGQGL
X. laevis   ATRNCLVGENL
D. rerio   ATRNCLVGEGL
G. gallus   ATRNCLVGHDL
D. melanogaster   AARNCLVNEGL
C. elegans   ATRNCLVGDTR

p.I699T   MPPESTLYRKF
H. sapiens   MPPESILYRKF
X. laevis   MPPESIMYRKF
D. rerio   MPPESIMYRKF
G. gallus   MPPESILYRKF
D. melanogaster   MPSESILYGKF
C. elegans   MSKEAIEQGRF

p.C752S   ERPRASPPEVY
H. sapiens   ERPRACPPEVY
X. laevis   QRPRTCPKEVY
D. rerio   ERPRTCPKEVH
G. gallus   ERPRTCPSEVY
D. melanogaster   SAPENCPTAVY
C. elegans   ECPHNCPTNIY

p.C763S   AIMRGSWQREP
H. sapiens   AIMRGCWQREP
X. laevis   ALMRGCWQREP
D. rerio   LLMQGCWQREP
G. gallus   DIMQSCWQREP
D. melanogaster   SLMIECWHEQS
C. elegans   SLMVECWHENI

p.R771C   KDVHACLQALA
H. sapiens   KDVHARLQALA
X. laevis   KEIHSLLQNLS
D. rerio   KDIYSRLVALV
G. gallus   QDIHSRLQALV
D. melanogaster   TDISNRLKTWH
C. elegans   SEIRSRLQSWS

B

Mutation	SIFT prediction score	Polyphen prediction score
p.G517E	0.00	1.000
p.G522E	0.00	1.000
p.L567P	0.00	0.983
p.I699T	0.00	0.953
p.C752S	0.00	1.000
p.C763S	0.00	1.000
p.R771C	0.00	1.000

C

481 GKGSGLQGHIIENPQYFSDACVHHIKRRDIVLKWELGEGA
521 FGKVFLAECHNLLPEQDKMLVAVKALKEASESARQDFQRE
561 AELLTMLQHQHIVRFFGVCTEGRPLIMVFEYMRHGDINRF
601 LRSHGPDAKLLAGGEDVAPGPLGLGQLLAVASQVAAGMVY
641 LAGLHFVHRDLATRNCLVGQGLVVKIGDFGMSRDIYSTDY
681 YRVGGRTMLPIRWMPPESILYRKFTTESDVWSFGVVLWEI
721 FTYGKQPWYQLSNTEAIDCITQGRELERPRACPPEVYAIM
761 RGCWQREPQQRHSIKDVHARLQALAQAPPVYLDVLG

| ATP binding domain	Activation loop
Active site	Catalytic domain

(A): The missense TRKA candidate mutations all resulted in the change of an evolutionary conserved amino acid. Protein sequence data are for human as a representative mammal (TKRA, NP_00252), *Xenopus laevis* for amphibians (NP 001079579.1), *Danio rerio* for fish (NP_001288285), *Drosophila melanogaster* for flies (NP_476962.1) and *Caenorhabditis elegans* as a nematode (NP_001033327.1). Multiple sequence alignment was performed using Clustl Omega. The candidate mutations are shown in black and the amino acid at that

position in the different species are shown in red. Any variance that occurs at this position is also shown in black.

(B): All of the missense mutations were predicted to be damaging and pathogenic by Polyphen, where most damaging is given a score of 1. These same mutations were also predicted to be damaging by SIFT with the lowest score of 0.

(C): The identified residues are all within in subdomains of the tyrosine kinase domain of TRKA as shown.

Supplementary Figure S4: Colocalization of TRKA with Na$^+$/K$^+$ ATPase
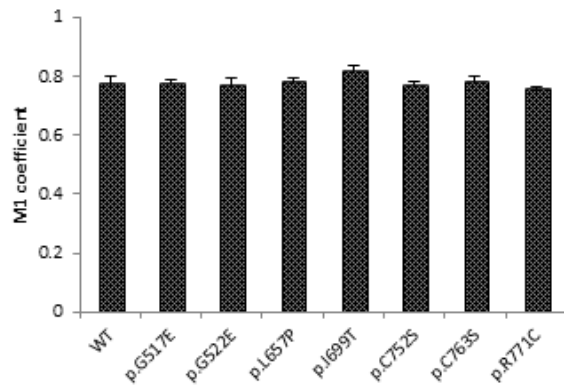
Colocalization of TRKA at the periphery of the cells with the plasma membrane Na$^+$/K$^+$ ATPase was determined in terms of the Manders M1 coefficient. Wild-type TRKA was found to colocalize with the plasma membrane as were all the mutant TRKA proteins. WT: wild-type.

Supplementary Figure S5: Activation of the PLCγ pathway by TRKA mutants
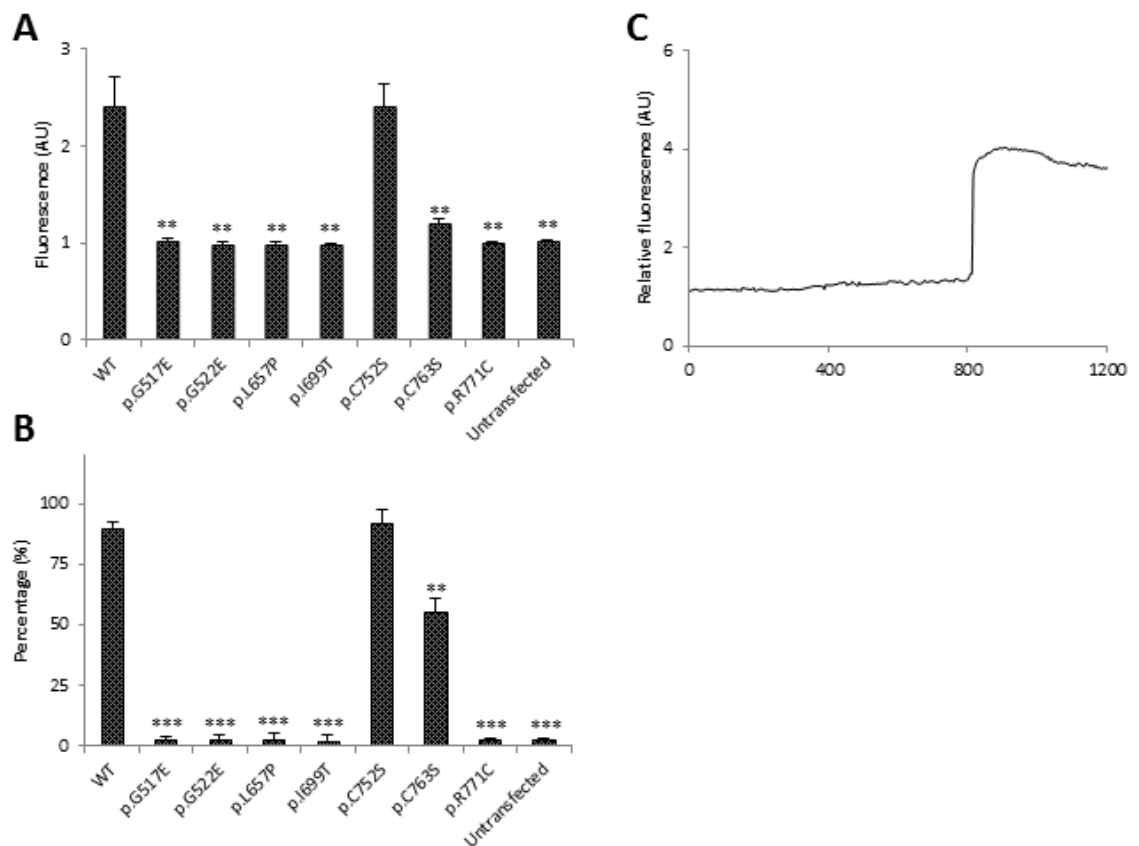
(A): HeLa cells were transfected and the calcium levels were monitored after NGF application. Fluorescence at t= 208 s was quantified. The maximum fluorescence in C752S transfected cells was not different from the maximum fluorescence of wild-type transfected cells. Maximum fluorescence was reduced 2-fold in C763S transfected cells and in all the other mutants it did not increase above baseline levels. WT: wild-type.

(B): The percentage of cells with a calcium response was determined. Any cell that had a relative fluorescence greater than 15% of the baseline after NGF addition was classified as a responsive cell. A 90% of wild-type and C752S cells had a calcium response, whereas this was reduced in C763s transfected cells and was almost 0% in all the other mutants.

The bar graphs in A and B represent the mean values of n= 3, with around 15 cells in each repeat, and error bars represent standard error of the mean. Statistical differences between wild-type and mutant TRKA are indicated as **P<0.01 or ***P<0.001 (one-way ANOVA, followed by Student's t test using a Bonferroni adjusted P-value).

(C): WT transfected HeLa cells were treated with 3 µM of U73122, a phospholipase C inhibitor for 30 min. After incubation, the NGF induced increase in fluorescence was inhibited.

Supplementary Table S1: Summary of functional characterization of previously identified TRKA

mutations

Mutation	Full glycosylation	Membrane expression	Autophos-phorylation	Y496 phos-phorylation	PLCγ activation	Neurite outgrowth
p.L93P	Abolished	—	Abolished	Abolished	—	—
p.L213P	Abolished	Null	Abolished	Abolished	—	Abolished
p.G516R	No effect		Abolished	Abolished	—	—
p.G571R	—	No effect	Abolished	Abolished	—	Abolished
p.R643W	No effect	—	Abolished	Abolished	—	Abolished
p.R648C	No effect	—	Abolished	Abolished	—	—
p.G708S	No effect	—	Abolished	Abolished	—	Abolished
p.R774P	—	—	Abolished	—	—	—

Functional characterization of previously published mutations identified these as functional nulls, where kinase activity was abolished. In most cases Y496 phosphorylation was also investigated as was the presence of the fully glycosylated form.

Supplementary Table S2: Summary of phenotype of patients

Case	*NTRK1* mutations	TRKA protein	Age at diagnosis	Ethnicity and sex	Congeital analgaesia	Sweating	Temperature sensing/ episodes of hyperthermia	Itching/ and licheni-fication	Cognition	Staphylococcal Aureus infections/ Charcot's joints
1	Het c.1550G>A, c.717+4A>T[a]	p.G517E, Null	15y	Caucasian, male	Yes	None	None/No	No/No	Mild cognitive delay	Yes/yes
2	Het c.1565G>A, c.2254T>A	p.G522E, p.C752S	8y	Caucasian, female	Yes	None	None/No	Yes/No	Mild cognitive delay	Yes/ No
3 and 4	Homozygous c.1970T>C	p.L657P	10y and 3y	Pakistani*, female and male	Yes	None	None/No	Yes/Yes and Yes/No	Moderate cognitive delay and ?	Yes/Yes and Yes/No
5	Het c.2096T>C, c.287+2 dupT[b]	p.I699T, Null	3y	Pakistani, male	Yes	None	None/Yes	Yes/No	Mild cognitive delay	Yes/No
6	Homozygous c.2288G>C	p.C763S	6y	Turkish*, Male	Yes	None	None/Yes	Yes/No	Mild cognitive delay	Yes/No
7	Homozygous c.2311C>T	R771C	8y	Indian*, male	Yes	None	None/Yes	Yes/Yes	Moderate cognitive delay	Yes/No

Nucleotide numbering uses +1 as the A of the ATG translation imitation codon in the reference sequence, with the initiation codon as

codon 1 (RefSeq ID NM_002529.3, NP_002520) .

a. Alters an evolutionary conserved splice donor site of intron 6 from gGTAAT to gGTATT, where the +4 A is conserved in all species with a NTRK1 gene. Of note the spice acceptor for this intron 5 of NTRK1 is predicted as poor TAACACCCCTTGGCCCTCGGCGTCCTGGGTGGCCAGg. MIT splice predictor, SplicePort and NetGene2 – do not predict the proven NTRK1 intron 5 acceptor splice site.

b. Changing the splice donor site from tGTGAG to tGTTGAG; previously reported as pathogenic in Lee ST et al, Muscle Nerve, 2009, 40(5):855-9)

*. Parents consanguineous.